cryo

MDPI

Review

Development of Cryogenic Structural Steels for Magnetic Confinement Fusion

Jingjing Dai [1,2] and Chuanjun Huang [1,*]

[1] Technical Institute of Physics and Chemistry, Chinese Academy of Sciences, Beijing 100190, China; daijingjing22@mails.ucas.ac.cn
[2] University of Chinese Academy of Sciences, Beijing 100049, China
* Correspondence: cjhuang@mail.ipc.ac.cn

Abstract

With the growth in global energy demand and increasing concern over the environmental issues associated with fossil fuels, magnetic confinement fusion (MCF) has gained widespread attention as a clean and sustainable energy solution. The superconducting magnet systems in MCF devices operate under liquid helium temperature of 4.2 K and strong magnetic fields, requiring structural materials to possess exceptional high strength, high toughness, and non-magnetic properties. This paper reviews recent research advances in cryogenic high-strength and high-toughness austenitic stainless steels (ASSs) for MCF devices, focusing on modified grades like 316LN and JK2LB used in the International Thermonuclear Experimental Reactor (ITER) project, as well as China's CHN01 steel developed for the China Fusion Engineering Test Reactor (CFETR) project. The mechanical properties at 4.2 K (including yield strength ($R_{p0.2}$), fracture toughness ($K(J)_{Ic}$), and Elongation (e)), microstructural evolutions, weldability, and manufacturing challenges of these materials are systematically analyzed. Finally, the different technical approaches and achievements in material development among Japan, the United States, and China are compared, the current limitations of these materials in terms of weld integrity and manufacturability are discussed, and future research directions are outlined.

Keywords: magnetic confinement fusion; International Thermonuclear Experimental Reactor; China Fusion Engineering Test Reactor; cryogenic structural steels; mechanical properties; CHN01 austenitic stainless steel

check for updates

Academic Editor: Laura Savoldi

Received: 9 July 2025
Revised: 18 September 2025
Accepted: 11 October 2025
Published: 30 October 2025

Citation: Dai, J.; Huang, C. Development of Cryogenic Structural Steels for Magnetic Confinement Fusion. *Cryo* **2025**, *1*, 13. https://doi.org/10.3390/cryo1040013

Copyright: © 2025 by the authors. Licensee MDPI, Basel, Switzerland. This article is an open access article distributed under the terms and conditions of the Creative Commons Attribution (CC BY) license (https://creativecommons.org/licenses/by/4.0/).

1. Introduction

The global energy crisis driven by population growth and industrialization has exposed the limitations of fossil fuels, namely, volatile supply chains and catastrophic greenhouse gas emissions [1]. Fusion energy emerges as an alternative solution by fusing deuterium (D) and tritium (T) to helium (He) and a neutron at extremely high temperatures, offering a clean and virtually waste-free energy source [2].

Primary terrestrial approaches for controlled fusion are inertial confinement (laser-driven pellet compression) and magnetic confinement (using magnetic fields). Among these, magnetic confinement, particularly the tokamak design, represents the most mature and dominant pathway towards practical fusion power. Invented in the 1950s at the Kurchatov Institute, the tokamak is a toroidal device whose key enabling systems for plasma confinement include a vacuum chamber, a magnet system, and the structural supports that must withstand immense electromagnetic forces [3]. Tokamak devices create

the conditions for fusion reactions by controlling high-temperature plasma through a powerful magnetic confinement system. The International Thermonuclear Experimental Reactor (ITER), as a collaborative effort among the Europe, the United States, Russia, Japan, China, South Korea, and India, aims to prove the feasibility of fusion for large-scale energy production. Parallel breakthroughs include the Toroidal Fusion Test Reactor (TFTR) in the US, which pioneered plasma confinement techniques [4]. Japan demonstration (JA-DEMO) in Japan and K-DEMO in South Korea target commercial reactor designs [5,6]. The Experimental Advanced Superconducting Tokamak (EAST) in China achieved a world-record high confinement plasma operation with a 403-s steady state in 2023 [7,8]. Notably, the China Fusion Engineering Test Reactor (CFETR) bridges experimental goals of the ITER with the commercialization roadmap of DEMO.

The ITER magnet system integrates four magnet systems, comprising Central Solenoid (CS) coils, which generate inductive current for plasma initiation, Toroidal Field (TF) Coils which confine plasma through a helical magnetic field, and Polar Field (PF) and Correction (CC) Coils, which finely tune plasma positioning and stability. These coils demand extreme currents up to 95.6 kA for TF coils and 60 kA for CS coils and magnetic fields as high as 17 T and 14.5 T in advanced devices like the CFETR to achieve fusion-grade plasma parameters [9,10]. Such conditions necessitate superconducting materials (Nb_3Sn and NbTi) to eliminate resistive losses and enable ultra-high current densities. The chosen conductor architecture is the Cable-In-Conduit Conductor (CICC), wherein the superconducting cables are housed within a structural conduit and cooled by supercritical helium to maintain cryogenic stability. As illustrated in Figure 1, the CICCs used in different coils exhibited significant variations in terms of dimensions, cross-sectional configurations, and the layout of superconducting cable bundles. These structural variations directly influence the electromagnetic forces imposed on the ASS jackets, the manufacturing complexities, and the mechanical performance requirements. Consequently, a range of high-performance steels has been developed to meet these specific demands.

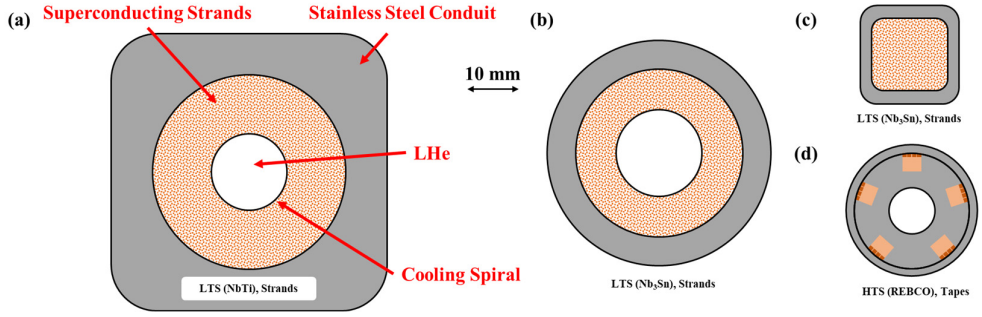


Figure 1. Cross-section of several conductors designed in the ITER: (**a**) PF of the ITER; (**b**) TF of the ITER; (**c**) CC of the ITER; (**d**) CICC for High-Temperature Superconducting (HTS) by ENEA (Note: this conductor is shown for comparative purposes as an example of next-generation HTS technology).

Austenitic stainless steels (ASSs), renowned for their excellent properties including high strength, high toughness, and non-magnetic at cryogenic temperatures, have become crucial structural materials for jackets of the CICCs and cases of coils in many large-scale and high-field tokamaks. However, traditional alloys like Fe-Mn-Cr and Fe-Ni-Cr steels faced a severe challenge posed by the requirement of withstanding huge electromagnetic forces while retaining sufficient ductility at 4.2 K [11]. Japan pioneered Fe-Mn-Cr alloys by optimizing Cr and Ni content (such as 25Cr-13Ni-0.4N and 27Cr-18Ni-0.35N), successfully enhancing nitrogen solubility for solid-solution strengthening while suppressing embrittlement [12]. The ITER has established the baseline for cryogenic structural steels; however, next-generation MCF devices demand even higher strength-toughness combinations and enhanced resistance to cyclic loading. Building on advancements that have already been made, China has initiated

a program since 2015 to develop next-generation ASS for next-generation MCF projects, and a landmark achievement was the CHN01 steel, engineered by the Technical Institute of Physics and Chemistry (TIPC, CAS) in collaboration with the Hefei Institute of Physical Science (HFIPS, CAS). Unique composition of the CHN01 steel combining refined Cr/Ni ratios and nitrogen microalloying enabled outstanding cryogenic performance with $R_{p0.2}$ exceeding 1500 MPa and $K(J)_{Ic}$ more than 200 MPa·m$^{1/2}$ at 4.2 K. The CHN01 steel was officially selected for the superconducting magnet system of the Burning Experimental Superconducting Tokamak (BEST) in 2022.

This paper comprehensively reviews recent advancements in cryogenic high-strength and high-toughness ASSs, which are critical for MCF devices. We highlight the important role of ASSs in superconducting magnets for the ITER, the CFETR, and the JA-DEMO, including the modified 316LN, JK2-Low C-B-added (JK2LB), JJ1, and the CHN01. Key discussions include mechanical performance under extreme conditions, phase stability, and fabrication challenges, alongside comparative analyses of international R&D efforts in Japan, the United States, and China. This paper underscores the significance of advanced structural ASSs in enabling sustainable fusion energy, and provides a reference for future research to bridge gaps between laboratory-scale achievements and industrial- scale for future commercial fusion reactor demands.

2. Austenitic Stainless Steels for the ITER Superconducting Magnets

2.1. Jackets of the CICCs of Coils

The ITER magnets consist of 18 TF coils, 6 individually powered CS coils, 6 PF coils, and 18 CC coils [13]. The distribution of manufacturing responsibilities for jackets of CICC of coils in the ITER coil is detailed in Table 1. China was responsible for 7.51% of jackets of the TF coils, 67% of jackets of the PF coils (PF 2/3/4/5), and 100% of jackets of the CC coils. The ITER project has developed a variety of cryogenic structural steels, among which the modified 316LN, JK2LB, modified 316L, and 316L steel were selected as the jackets of the CICCs of the TF coils, the CS coils, the PF coils, and the CC coils, respectively. Their chemical compositions and mechanical properties are displayed in Tables 2 and 3. It should be noted that while the official ITER specification sets a maximum cobalt content limit of 0.1 wt.% [14], the actual levels in produced steels are typically maintained within a much stricter range of 0.01 to 0.06 wt.% [15]. A comparative analysis of the mechanical properties in Table 3 reveals that all ITER-grade steels meet or significantly exceed the project's specifications at 4.2 K. For instance, the JK2LB (CS coils) achieves an exceptional K_{Ic} of 209 MPa·m$^{1/2}$, far above the requirement of 130 MPa·m$^{1/2}$. Notably, the newly developed CHN01 steel targeting the CFETR, demonstrates superior performance with a yield strength of 1600 MPa and $K(J)_{Ic}$ of 265 MPa·m$^{1/2}$, setting a new benchmark for next-generation reactors.

The modified 316LN austenitic stainless steel has been adopted for the jackets of CICCs of TF coils due to its exceptional mechanical performance at cryogenic temperatures and non-magnetic properties [16]. Extensive studies [17–21] on sub-sized and full-scale samples confirm that its mechanical performance at 4.2 K including a $R_{p0.2}$ exceeding 950 MPa, e greater than 20%, and K_{Ic} over 150 MPa·m$^{1/2}$, meets ITER's specifications even after compaction and aging treatments. The high nitrogen and low carbon content in modified 316LN significantly enhanced $R_{p0.2}$ and R_m for metastable ASS without significant impact on the total e at cryogenic temperatures [22]. In general, increased cold working elevated the $R_{p0.2}$ at 4.2 K of both base material and weldments but reduced e [23–25]. Conversely, those subjected to cold working and aging treatment exhibited an improvement in e from 37% to 41% and from 23% to 38%, respectively [26,27]. Short-duration Nb_3Sn reaction heat treatments (625 °C for $\leq$100 h) showed no detrimental effect on the cryogenic me-

chanical properties of modified 316LN. In contrast, prolonged aging treatments (625 °C for 696 h) have been found to be able to further improve strength [18,20,28]. A significant challenge arose from the ultrathin thickness of jackets (~2 mm), which prevented standardized K_{Ic} and fatigue crack growth rate (FCGR) tests. Researchers replaced K_{Ic} with a ductility-based criterion (*e* more than 20% below 7 K) and evaluated grain boundary sensitization through fracture surface analysis [29]. While the ductility-based criterion provided a practical workaround for quality control, it remains an indirect and potentially less conservative measure of fracture resistance compared to direct K_{Ic} measurement. The critical gap between standardized evaluations and real-world constraints of thin-walled jackets could be solved by more sophisticated and non-destructive evaluation techniques (such as Acoustic Emission [30]). These practical challenges have intensified research into the microstructural origins of fracture in modified 316LN. However, clear contradictions existed in the literature: some studies using EBSD and TEM confirmed the presence of strain-induced $\gamma \rightarrow \alpha'$ martensitic transformation at cryogenic temperatures and high deformation levels [19,21,31,32], while others, employing similar techniques, reported no martensite formation and attributed deformation structures solely to dense dislocation networks and stacking faults [17,33–37]. Notably, magnetic data have suggested that the amount of α'-martensite decreased in a linearly proportional manner from the fracture origin to the root on the parallel section [25,38,39]. This obvious discrepancy cannot be dismissed as mere observational error and suggests that subtle differences in material processing, thermomechanical history, or local compositional gradients may critically influence the deformation mechanism of modified 316LN. Resolving this inconsistency is essential for a predictive understanding of fracture behavior and requires systematic reinvestigation under carefully controlled and documented conditions.

Table 1. Production proportions of each country for coils in the ITER (Data from [40]).

		TF	CS	PF1&6	PF2–5	CC
Assignment proportion (%)	CN	7.5			100	100
	EU	20.2		39.8		
	JA	25.0		60.2		
	KO	20.2				
	RF	19.3				
	US	7.8	100			

Table 2. Chemical compositions (wt%) and size of jackets of the CICCs of the ITER (Data from [14,15]).

		TF	CS	PF1&6	PF2–5	CC
Material types		Modified 316LN	JK2LB	Modified 316L		AISI 316L
Chemical compositions (wt%)	C	<0.015	<0.02	≤0.03		≤0.03
	Si	<0.75	<0.28	≤0.75		≤0.75
	Mn	<2.0	20.50–22.50	≤2.00		≤2.00
	P	<0.04	<0.008	≤0.03		≤0.045
	S	<0.03	<0.008	≤0.01		≤0.030
	Cr	16.0–18.0	12.00–14.00	16.00–18.50		16.0–18.0
	Ni	11.0–14.0	8.0–10.0	11.0–14.0		10.0–14.0
	Mo	2.0–3.0	0.5–1.5	2.00–2.50		2.00–3.00
	N	0.14–0.18	0.09–0.15			0.1–0.16
	B		0.001–0.004			
	Co	<0.1	<0.1	≤0.1		
Coil shapes		Circle	Circle in square	Circle in square		Square
Coil sizes (mm)	Outer diameter	43.7	49.0	53.8	51.9	19.2
	Inner diameter	39.7	32.6	37.7	35.3	14.8

Table 3. Mechanical properties of jackets of CICCs of the coils in the ITER and CFETR at 4.2 K (Data from [15,41,42]) specification (real value).

		Modified 316LN	JK2LB	Modified 316L	316L	CHN01
Yield strength ($R_{p0.2}$) (MPa)	4.2 K	>950 (1165)	>850 (1076)	>700 (797)	>700 (813)	>1500 (1600)
	300 K	(530)	>700 (800)	>173 (494)	>173 (512)	547
Tensile strength (R_m) (MPa)	4.2 K	(1537)	>1150 (1450)	>1000 (1525)	>1000 (1582)	>1800 (1930)
	300 K	(746)	>1000 (1550)	>483 (626)	>483 (615)	>480 (776)
Young's modulus (E) (GPa)	4.2 K	(202)	(201)	>205 (209)	(202)	(216)
	300 K	(195)	>180 (192)	>190 (193)	>190 (194)	(184)
Elongation (e) (%)	4.2 K	>20 (34)	>25 (43)	>40 (45)	>30 (39)	>25 (34)
	300 K	(38)	>30 (44)	>35 (51)	>35 (45)	>35 (50)
Fracture toughness ($K(J)_{Ic}$) (MPa·m$^{1/2}$)	4.2 K	>150 (300)	>130 (209)	>150 (278)		>130 (265)
Pre-test processing		Compaction 3.5%; Tensile 2.5%; 650 °C (200 h)	Compaction 3.5%; Tensile 2.5%; 650 °C (200 h)	Compaction 5%; Bending (radius 2 m); Straightening	Compaction 3.5%; Tension 2.5%	Compaction 5%; Bending (radius 2 m); Straightening; 665 °C (50 h)

The CS coils critical for plasma current induction and shaping in tokamaks demand jackets that can balance cryogenic strength, fatigue resistance, and dimensional stability under extreme cyclic loading. In response to these stringent demands, the Japan Atomic Energy Agency (JAEA) and Kobe Steel developed JK2LB steel, a low-carbon, low-boron, nitrogen-strengthened ASS (0.03C-22Mn-13Cr-9Ni-1Mo-0.24N-B), as a superior alternative to conventional 316LN steel. Its reduced thermal shrinkage (0.21% vs. 0.29% for 316LN) provides critical thermal compatibility by minimizing compressive stresses on the brittle Nb_3Sn strands during cooldown and operation [43–46]. The mechanical performance of JK2LB at 4.2 K is profoundly influenced by its thermal-mechanical processing history. While cold working prior to heat treatment could enhance subsequent precipitation hardening (18.5% cold working increasing $R_{p0.2}$ from 1007 MPa to 1442 MPa but reducing K_{Ic} from 144.1 MPa·m$^{1/2}$ to 52.3 MPa·m$^{1/2}$ [47,48]), specific optimized heat treatments (570 °C for 250 h and 650 °C for 100 h) have been developed to maintain high ductility (e > 30%) without decreasing strength [49]. This tailored approach was underpinned by microstructural optimizations, including reduced carbon (<0.03%) and controlled nitrogen (~0.2%) content, which suppressed detrimental chromium carbide ($Cr_{23}C_6$) precipitation and mitigated aging-induced embrittlement [50,51]. As a result, even after compaction and aging treatments, JK2LB maintains a $R_{p0.2}$ exceeding 850 MPa and K_{Ic} above 130 MPa·m$^{1/2}$ [47,49–55]. Moreover, JK2LB ensured functional reliability through its antiferromagnetic behavior below 240 K, which guaranteed compatibility with high superconducting fields. JAEA implemented a rigorous non-destructive examination (NDE) regime for jackets of CS coils to ensure the integrity of the manufactured jackets against even minuscule defects that could initiate fatigue cracks under 60,000 operational cycles [56]. NDE system employs two complementary techniques: Eddy Current Testing (ECT) for detecting surface flaws on both the inner and outer jacket surfaces, and Phased Array Ultrasonic Testing (PAUT) for identifying embedded volumetric defects. The inspection criteria are based on a linear elastic fracture mechanics (LEFM) analysis, setting the maximum allowable defect size at 2 mm^2 for surface flaws and between 5 and 7 mm^2 for internal defects, depending on their location. NDE has been successfully validated on over a thousand jacket sections, demonstrating the capability to reliably detect critical flaws and ensuring the functional reliability of every production unit [57]. Together, these excellent thermal and mechanical properties establish JK2LB as a comprehensively engineered ASS capable of meeting the integrated demands of CS coil operation.

The PF magnet system consists of six poloidal coils from PF1 to PF6, which are connected to the outside of the TF coil box by flexible plates or sliding supports to stabilize the positional equilibrium of the plasma current and the vertical stability of the plasma [58].

For the critical PF2 to PF5 coils, a modified 316L steel was selected for the CICC jackets due to its balanced mechanical properties. To accurately simulate in-service conditions, the modified 316L steel underwent rigorous processing, including compaction, bending, and straightening, prior to comprehensive mechanical evaluation. Performance assessments across a range of temperatures (4.2 K, 77 K, and 300 K) confirmed that the modified 316L steel met ITER's stringent requirements for tensile strength, impact toughness, and fatigue resistance [59–61]. Detailed investigation revealed that a 5.58% compaction treatment induced a strain-driven $\gamma \rightarrow \alpha'$ martensitic transformation, which enhanced $R_{p0.2}$ by 10% and improved impact toughness at 4.2 K. However, the strengthening mechanism came at the expense of ductility, with e reduced by 4% due to concurrent dislocation slipping and stacking fault formation [60,61]. Both the PF and CS coil jackets employed a combined strategy of Phased Array Ultrasonic Testing (PAUT) and Eddy Current Testing (ECT) for NDE. However, a specialized NDE procedure has been developed for the modified 316L jackets of the PF coils, accounting for their complex circular-in-square cross-section. The PAUT method utilized four different probes and performed 11 separate scans over each jacket surface to reliably identify internal volumetric defects, while multi-frequency ECT was specifically employed to detect transverse inner surface flaws with depths of up to 2–3 mm. The NDE for modified 316L jackets has achieved a high acceptance rate of 96.3%, providing essential quality assurance for conductor assembly. Note that the allowable defect sizes are larger (10 mm^2 for surface defects and 20 mm^2 for embedded defects at the corners) compared to those specified for the JK2LB jackets [62]. The NDE methodology can be extended and refined for next-generation MCF devices (CFETR), whose TF coils will face even greater electromagnetic loads and require higher-performance materials (CHN01 steel). The experience gained in inspecting complex geometries and qualifying stringent acceptance criteria is directly applicable to developing the inspection protocols for CFETR's larger and more robust conduits, ensuring their reliability under more extreme operational conditions. Notably, the magnetic permeability, a critical parameter for non-magnetic fusion components, remained uncharacterized in these studies. Given that the formation of ferromagnetic α'-martensite could compromise the material's non-magnetic performance, future research must comprehensively evaluate its magnetic characteristics to ensure full compliance with fusion application standards.

The CC coils comprise six Top Correction Coils (TCCs), six Bottom Correction Coils (BCCs), and six Side Correction Coils (SCCs) to compensate for field errors arising from manufacturing deviations, assembly tolerances, and winding distortions [63]. To ensure mechanical reliability under cyclic electromagnetic loads in this critical system, 316L steel was selected as the jacket material for the Cable-In-Conduit Conductors (CICCs) owing to its outstanding cryogenic performance, which includes a $R_{p0.2}$ exceeding 700 MPa and e greater than 35% at 4.2 K [64,65]. High strength coupled with exceptional ductility provides a critical foundation for resisting fatigue cracking in high-field environments. The high strength enables the material to withstand the significant cyclic stresses inherent to coil operation, while the superior ductility allows it to absorb deformation energy and mitigate crack initiation and propagation. However, while these tensile properties are strong indicators of fatigue resistance, the direct measurement of fatigue life under the relevant stress ranges (300–600 MPa) remains an essential objective for future validation to fully confirm the 316L's performance for long-term operation.

2.2. Cases of the TF and CC Coils

For the cases of TF and CC coils of the ITER, the production tasks have been entirely undertaken by Japan and China, respectively. JJI and 316LN steel have been developed and utilized as materials for the coil cases, whose chemical compositions and mechanical

properties are presented in Tables 4 and 5. The compositional difference between JJ1 (TF coils) and 316LN (CC coils) was revealed in Table 4, which was referred to as high-Mn, high-Mo and high-N grade (9–11% Mn, 4–6% Mo, 0.21–0.27% N) were designed for JJ1.

The cases of the TF coils, designed to mechanically protect TF superconducting windings [66], endure severe in-plane static and out-of-plane cyclic stresses, particularly at the inward bending regions during Tokamak operation [67]. Material selection for this critical component prioritizes high strength, fatigue resistance, and weldability at 4.2 K, with Quantum Science and Technology (QST) recommending JJ1 steel for high-stress zones and graded 316LN variants including 316LNH (C + N $\geq$ 0.18%), 316LNM (C + N $\geq$ 0.13%), and 316LNL (C + N $\geq$ 0.08%) for moderate to low stress areas [68]. <JSME Codes for Fusion Facilities> was established for JJ1 and 316LN variants to reduce the high cost of cryogenic testing, mainly containing prediction curves for $R_{p0.2}$ and R_m at 4 K based on the (C + N) content and mechanical properties at 300 K [69,70]. Over 2400 materials were tested and registered, validating the approach despite an inherent scatter of $\pm$10% in predictions. A detailed assessment of the reasons for the scattered values and how the values can be improved is a subject for a future study. However, the mechanical performance of its weld was constrained by geometric size sensitivity (miniaturized specimens showed crooked crack propagation) and welding-induced embrittlement. Narrow-gap tungsten inert gas welding (NG-TIGW) with a specially matched filler metal (Table 4) has been employed to enhance joint uniformity and strength by reducing inclusions [71]. Further studies showed that EBW was applicable but limited to 40 mm thickness, with vertical upward EB welding being the preferred method [72,73]. Nevertheless, aging treatments were found to promote detrimental carbide ($M_{23}C_6$) and nitride (Cr_2N) precipitation, underscoring the need for careful thermal process control to avoid intergranular embrittlement [74,75]. In contrast, the 316LN variants demonstrated superior ductility (e >50%) critical for components under cyclic electromagnetic loads. And their welded joints exhibited sufficient safety margins under cyclic loading, as reflected in S-N curve performance [76,77]. This presents a fundamental design choice: JJ1 offers superior base metal toughness but requires meticulous control over welding and heat treatment, while 316LN variants provide more predictable weldability and reliability.

Table 4. Production countries and chemical compositions of TF and CC cases in the ITER (wt%) (Data from [69,75,76,78]).

		CASE of TF					**CASE of CC**	
Assignment proportions (%)	CN						100%	
	JA		100%					
Material types		JJ1	Filler material	316LNH	316LNM	316LNL	316LN	Filler material
Chemical compositions	C	<0.03	0.016	<0.03	<0.03	<0.03	<0.03	0.018
	Si	<0.75	0.52	<0.75	<0.75	<0.75	<1.0	0.46
	Mn	9.0–11.0	10.17	<2.0	<2.0	<2.0	<2.0	7.01
	P	<0.035	0.004	<0.03	<0.03	<0.03	<0.04	0.017
	S	<0.015	0.004	<0.02	<0.02	<0.02	<0.03	0.003
	Cr	11.0–13.0	12.27	16.0–18.5	16.0–18.5	16.0–18.5	16.0–18.0	20.59
	Ni	11.0–13.0	14.16	10.0–14.0	10.0–14.0	10.0–14.0	10.0–14.0	15.37
	Mo	4.0–6.0	4.97	2.0–3.0	2.0–3.0	2.0–3.0	2.00–3.00	2.83
	N	0.21–0.27	0.162	0.17–0.22	0.12–0.17	0.10–0.12	<0.18	0.156

Table 5. Mechanical properties of cases of TF and CC cases in the ITER (Data from [68,76,79,80]) specification (real value).

		JJ1	**316LNH**	**316LNM**	**316LNL**	**316LN**
Yield strength ($R_{p0.2}$) (MPa)	4.2 K	>1000 (1126)	>900 (1093)	>700 (868)	>500 (713)	>700 (1080)
	300 K	(330)	(355)	(289)	(263)	>250 (318)

Table 5. *Cont.*

		JJ1	316LNH	316LNM	316LNL	316LN
Tensile strength (R_m) (MPa)	4.2 K	(1319)	(1444)	(1348)	(1313)	>1000 (1430)
	300 K	(665)	(666)	(590)	(557)	>480 (642)
Elongation (e) (%)	4.2 K	(42)				>35
	300 K	(65)				>40
Fracture toughness ($K(J)_{Ic}$) (MPa·m$^{1/2}$)	4.2 K	>200 (366)			>200	>180 (213)

The main characteristics of cases of the CC coils are compact cross-section (~240 mm × 147 mm), large overall dimensions (~7 m), and complex geometry (60° bend angle with an 8 m radius), which are used to strengthen the windings and thus to reduce the stress and deformation induced by electromagnetic loads [79,81]. The cases of the coils are constructed from 20-mm-thick 316LN ASS, chosen for its exceptional cryogenic strength and ductility [80]. The 316LN ASS must comply with rigorous cryogenic standards, including the $R_{p0.2}$ at 4.2 K, which should be more than 700 MPa, the R_m should be more than 1350 MPa, the e should be more than 40%, the K_{Ic} should be more than 180MPa·m$^{1/2}$, and the fatigue strength under 3000 cycles must be more than 500 MPa. Additionally, the welds of cases should satisfy that the $R_{p0.2}$ at 300 K should be more than 250 MPa, the R_m should be more than 480 MPa, and the K_{Ic} should be more than 180 MPa·m$^{1/2}$ [82,83]. Due to the strict manufacturing tolerances, tungsten inert gas (TIG) welding was employed for sub-assembly, while laser beam welding (LBW) was used for the final enclosure welding. This combination ensures full penetration and minimizes defects [84]. Due to the strict manufacturing tolerances, tungsten inert gas (TIG) welding was employed for sub-assembly, while laser beam welding (LBW) was used for the final enclosure welding. This combination ensures full penetration and minimizes defects [67]. The R_m of TIG and LBW weldments reached 1555 MPa and 1522 MPa at 4.2 K, respectively, representing 99.7% and 97.6% of the base material's strength. Both joints exhibit excellent ductility, with e exceeding 35%, and high $K(J)_{Ic}$ values of 210 and 241 MPa·m$^{1/2}$ [78,85,86]. The assembly process involves fabricating two L-shaped sections for the Side Correction Coil (SCC) and a U-shaped base with a planar cover for the Bottom/Top Correction Coils (B/TCC) [87]. The geometric complexity necessitates precise alignment to avoid residual stress concentrations.

The outstanding mechanical properties of these structure ASSs for fusion are intrinsically governed by their microstructural evolution under 4.2 K. The deformation mechanisms of face-centered cubic (FCC) metals are strongly influenced by their stacking fault energy (SFE), which depends strongly on deformation temperature and chemical compositions. As the temperature decreases from 300 K to cryogenic temperatures, the SFE is significantly reduced to activate nano-sized twinning and strain-induced martensitic transformation. Mechanical twinning tends to dominate within an intermediate SFE range (20 < SFE < 45 mJ·m^{-2}). When SFE falls below 20 mJ·m^{-2}, martensite formation ($\gamma \rightarrow \varepsilon$ and $\gamma \rightarrow \alpha'$) becomes the preferred deformation mechanism.; when SFE exceeds 45 mJ·m^{-2}, plastic deformation is controlled predominantly by dislocation glide [88,89]. For metastable austenitic alloys (modified 316L and 316LN), the strain-induced transformation of γ-austenite to α'-martensite provides a critical strengthening mechanism, though often causing an increase in magnetic permeability. In advanced nitrogen-alloyed steels (JK2LB and CHN01), high nitrogen content significantly increases phase stability by elevating SFE thereby preventing martensitic transformation. Dislocation and twinning formation are promoted ultimately to an exceptional combination of high strength and fracture toughness at cryogenic temperatures. Furthermore, the formation of nano-twins and phase boundaries strengthens the material by impeding dislocation

motion, resulting in high strain hardening rates (SHR) and simultaneously enhances both strength and ductility, a phenomenon known as the "dynamic Hall-Petch" effect [90]. These microstructural adaptations are essential for maintaining performance under the extreme operational conditions encountered in fusion magnet systems.

3. Historical Development of Cryogenic Structural Steels in Japan and the United States

3.1. Japan

In the 1980s, the Japan Atomic Energy Research Institute (JAERI) spearheaded the development of cryogenic structural steels for high-field superconducting magnets for the fusion devices. Domestic steelmakers (Nippon and Kobe Steel) achieved an unprecedented yield strength–fracture toughness balance ($R_{p0.2} \geq 1200$ MPa, $K(J)_{Ic} \geq 200$ MPa·m$^{1/2}$), known as the "JAERI-BOX" criterion, as shown in Figure 2 [91,92], which surpassed the limits of conventional AISI 300 series austenitic stainless steels. Through rigorous screening of over 80 candidate materials, including Ferritic Steels (FSs), High-Mn Austenitic Steels (HMASs), and others, as shown in Table 6, the Japanese Cryogenic Steels (JCS) series emerged [93], mainly high-Mn and nitrogen-strengthened CSUS-JN1/JK2 (22~24% Cr, 13~15% Ni, 0.2~0.3% N), optimized for higher $R_{p0.2}$ and R_m via solid-solution hardening, and low-Cr/Ni CSUS-JJ1 (12Cr-12Ni-5Mo-10Mn-0.2N), which excels in weldability and phase stability. Their chemical compositions are shown in Table 7. The JK2LB and JJ1 steels were ultimately selected for jackets of CICCs of the CS coils and cases of the TF coils in the ITER project due to their balanced cryogenic performance. Japan established a joint special design team in 2015 to enhance the coordination of JA-DEMO related research and development.

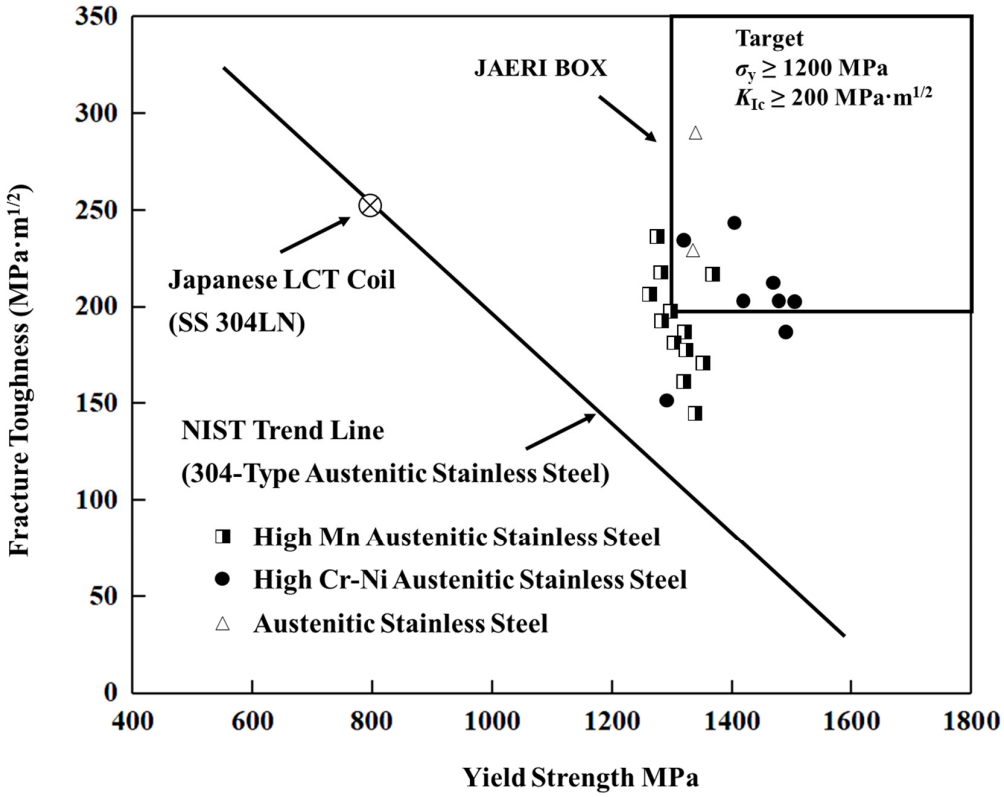


Figure 2. Relationship between fracture toughness and yield strength of JCS at 4.2 K.

Table 6. Development process of new cryogenic structural steels in JA and the USA.

Steps	Experiments	Requirements	Number of Test Steels at 4.2 K					Time
			ASS	HMASS	HMSS	FS	Total	
1	Tensile	$R_{p0.2} \geq 1200$ MPa and	31	40	14	4	89	1982
2	Charpy Impact	CVN ≥ 100 J	31	35	12	3	81	1984
	Next candidate materials		10	12			22	1986
3	Fracture toughness	$K_{Ic} \geq 200$ MPa·m$^{1/2}$	10	12			22	1988
4	Fatigue properties	~316LN	3	2			5	1990
	ITER candidate materials		1	1			2	

Table 7. Chemical compositions of the JCS.

JCS	C	Si	Mn	P	S	Ni	Cr	Mo	N	Cu	V
CSUS-JN1	0.026	0.99	4.2	0.026	0.002	14.74	24.2		0.34		
CSUS-JKA1	0.023	0.42	0.49	0.006	0.001	14.0	25.0	0.68	0.268		
CSUS-JN2	0.050	0.34	22.4	0.010	0.002	3.22	13.4	0.70	0.24	0.70	0.30
CSUS-JK2	0.05	0.36	21.79	0.013	0.005	4.94	12.82		0.212		
CSUS-JJ1	0.046	0.44	9.74	0.020	0.002	11.92	12.21	4.89	0.203		

3.2. The United States of America

The Massachusetts Institute of Technology (MIT) and International Nickel Corporation (INC) jointly developed an age-hardened nickel-based alloy, INCOLOY 908 [94], whose chemical compositions and mechanical properties of the INCOLOY 908 could be found in Tables 8 and 9. INCOLOY 908 showed excellent mechanical properties at 4.2 K: $R_{p0.2}$ increased to 1200 MPa and K_{Ic} increased to 200 MPa·m$^{1/2}$; however, FCGR was faster than that of modified 316LN steel [95]. The thermal shrinkage of the INCOLOY 908 alloy from 923 K down to 4.2 K is 1.1% (close to 0.7% for Nb_3Sn), which allows for higher pre-strain in Nb_3Sn strands; however, the INCOLOY 908 alloy carries the risk of stress-accelerated grain boundary oxidation (SAGBO) during heat treatment, and ultimately the ITER project abandoned the application of the INCOLOY 908 in the jacket of CICCs of the CS coils. The problem of SAGBO was avoided by vacuum heat treatment when applied to the jacket of CICCs of the CS coils in the KSTAR [96,97].

Table 8. Chemical compositions of the INCOLOY 908 (wt%) (Data from [98]).

Fe	Ni	Cr	Nb	Ti	Al	N	Mn	C	Co
40.7	49	3.98	2.92	1.74	0.93	0.002	0.041	0.01	<0.1

Table 9. Mechanical properties of the INCOLOY 908 for CICC tests (Data from [98]).

	Yield Strength ($R_{p0.2}$) (MPa)	Tensile Strength (R_m) (MPa)	Young's Modulus (E) (GPa)	Elongation (e) (%)	Fracture Toughness (K_{Ic}) (MPa·m$^{1/2}$)
4.2 K	1216	1694	177	22	196
300 K	1110	1302	171	22	196

4. Recent Advances in Austenitic Stainless Steels for Next-Generation MCF Devices

4.1. Japan

Japan proposed a conceptual design for a fusion demonstration reactor (JA-DEMO) in 2014, aiming to achieve stable power generation (fusion power (P_{fus} ~ 1.5 GW) and

validate commercial viability by the 2030s [99]. Transitioning to the engineering design phase around 2025, JA DEMO sets significantly higher technical benchmarks compared to the ITER, including larger aperture and enhanced magnetic field of the TF coils, as shown in Table 10. These demands place higher requirements on the cryogenic mechanical properties of structural steels in the JA-DEMO ($R_{p0.2}$ more than 1600 MPa and $K(J)_{Ic}$ more than 120 MPa·m$^{1/2}$ at 4.2 K) [100]. Japan is advancing next-generation nitrogen-strengthened austenitic steels, focusing on improving cryogenic strength.

Table 10. Comparison of the ITER and JA-DEMO.

	ITER	**JA-DEMO**
SC Strand	Nb_3Sn	Nb_3Sn
Number of TFC	18	16
B_{max}	11.8 T	13.9 T
Conductor current	68 kA	83 kA
Number of turns per TFC	134	192
Design stress	667 MPa	800 MPa
Total magnetic energy	41 GJ	153 GJ
Width/Height of TFC	8/12.6 m	12/19 m

Two advanced high-strength steels for JA-DEMO have been developed in Japan, i.e., an XM-19-derived Nb-containing material and a JN1-derived Nb-free material (chemical composition in Table 7) [101]. The ITER restricted Nb content to less than 0.05% due to irradiation embrittlement risks while Nb in XM-19 derivatives enhanced $R_{p0.2}$ through grain refinement. Fracture toughness evaluations revealed that the target of the JA DEMO aligns with a trend parallel to the reference line of the NIST, intersecting JN1's data points at $R_{p0.2}$ more than 1200 MPa and K_{Ic} more than 200 MPa·m$^{1/2}$ [101–103]. The chemical composition of the JN1 steel could be found in Table 6. Specimen No.1-3 can satisfy the performance target of the JA DEMO but exhibits unstable fracture risks as cracks terminate near specimen edges with minimal ligament retention. Consequently, the JA DEMO excludes Nb-containing steels for jackets of CICCs of TF coils, prioritizing Nb-free materials like JN1 derivatives to achieve high toughness ($K(J)_{Ic}$ > 120 MPa·m$^{1/2}$) [104]. Japan's prioritization of Nb-free steels for JA-DEMO, despite the attractive strength offered by Nb-containing grades, highlights a pivotal principle in fusion material development: prominent toughness is often more critical than marginal gains in strength. Any failure in a fusion magnet, often initiated from a microstructurally unstable region, can have catastrophic consequences, making reliability the paramount design criterion.

4.2. China

To bridge the gap between the ITER and the commercial fusion power plant, China plans to launch the CFETR project, aiming to establish the scientific and technological foundation for a fusion power plant prototype [1]. The primary objectives of CFETR include: (1) achieving a fusion power output of 50–200 MW; (2) sustaining effective full-power operation for 30–50% of the annual duty cycle; and (3) realizing tritium self-sufficiency through advanced neutron multiplication technologies in the breeding blanket [105,106]. To surpass the operational stability and power output of the ITER, the CFETR requires stronger magnetic fields (exceeding 13 T of the ITER) to confine high-energy plasmas, which imposes extreme mechanical demands on cryogenic structural steels. Specifically, the superconducting coils generate colossal cyclic electromagnetic forces, necessitating steels with $R_{p0.2}$ > 1350 MPa, R_m > 1650 MPa, e > 20% and $K(J)_{Ic}$ > 130 MPa·m$^{1/2}$ at 4.2 K [107]. The CHN01 (modified N50), a next-generation ultra-cryogenic austenitic stainless steel optimized for high strength and phase stability, has been developed [95].

This material exemplifies China's strategy to advance fusion engineering through tailored alloy design and rigorous performance validation.

Nitrogen-strengthened austenitic stainless steels were originally developed by Armco Steel at the beginning of the 21st century, and one of the most widely used nitro alloys is N50 (Nitronic 50, XM19, UNS S20910, 1.3964), which is a non-magnetic, corrosion-resistant, high-strength, and weldable (to a certain degree) nitrogen-strengthened austenitic stainless steel [108,109]. The N50 steel has been used in the form of large forgings of approximately 16 m in length for key connecting plate components of the ITER CS system [110], as shown in Figure 3. Figure 3 clearly demonstrates the full spectrum application potential of N50 and CHN01 steel, ranging from large-scale forgings (~16 m, Figure 3a) to medium-thickness coil boxes (~4.7 m, Figure 3b), and finally to ultra-thin jackets (~3 mm, Figure 3c), highlighting its versatility as the main structural material for the next-generation MCF devices. Initially, the N50 steel was used as a structural material without aging treatment and was strengthened with high carbon (0.06% max) and nitrogen (0.2–0.4%) contents. As a result, several problems arose during production including forging cracking during hot rolling and forging, carbide precipitation, and poor toughness.

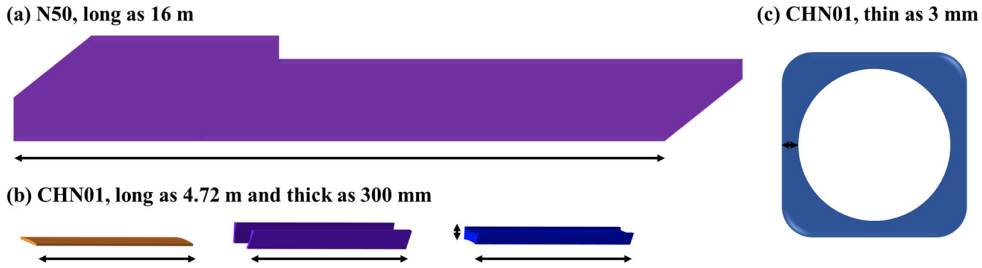


Figure 3. Schematic diagram of the application of large forgings: (**a**) N50, as a ~16 m long forging for key connecting plates in the ITER CS system; (**b**) CHN01, as a ~4.72 m long forging for casing components of the CFETR TF system; (**c**) CHN01, as a ~3 mm thin workpiece for jacket components of the CFETR TF system (Figure 3c has been enlarged ten times compared to its actual size to make it easier to view).

The CHN01 steel was then developed domestically by completely removing δ-ferrite and strictly controlling the carbon (max. 0.01%) and oxygen (max. 20 ppm) content [85,86]. Moreover, the content of nickel has been increased compared to that of the N50. Chemical compositions of the CHN01 and the N50 are shown in Table 11. These modifications made the CHN01 significantly different from the N50, characterized by excellent mechanical properties with the $R_{p0.2}$ of the CHN01 jacket after cold working and aging being about 1600 MPa, the e was more than 29%, and the $K(J)_{Ic}$ was more than 200 MPa·m$^{1/2}$ [42]. The CHN01 steel has been selected as a potential candidate for jackets of the CICCs of the TF and CS coils in the CFETR [95]. Further refinements, B microalloying (10 ~ 40 ppm) and δ-ferrite removal encouraged $K(J)_{Ic}$ by refining grain boundaries [111–113], while thermal deformation studies (950~1250 °C) revealed a transition from continuous to discontinuous DRX, guiding optimized hot-working processes [114]. The compatibility with ReBCO and Nb_3Sn conductors of the CHN01 jacket has been validated for the TF and CS coils in the CFETR [95,115].

Table 11. Chemical compositions of the N50 and CHN01 steel (Data from [116]).

	C	N	Cr	Ni	Mn	Mo	Nb	V	Si
N50 (XM-19)	0.058	0.30	23.23	13.5	4.81	2.08	0.22	0.25	0.67
CHN01	0.008	0.31	22.3	14.6	5.18	2.1	0.09	0.19	0.30

However, the performance of CHN01 welded joints remained a critical challenge for the application of Nb3Sn conductors despite the outstanding properties of the BM. The performance requirements for CHN01 welded joints in the CFETR are specified as follows: (1) a $R_{p0.2}$ > 1500 MPa and an e > 20%; (2) a $K(J)_{Ic}$ > 150 MPa·m$^{1/2}$ at 4.2 K. The Institute of Plasma Physics (ASIPP) employed tungsten inert gas welding (TIGW) to join CHN01 BM using CHN01J filler material [42]. Subsequent cryogenic tensile and fracture tests revealed that the CHN01 welded joints after Nb_3Sn ageing treatment exhibited degradation of $R_{p0.2}$, e, and $K(J)_{Ic}$ compared with that of CHN01 BM, as shown in Table 12, which could be attributed to the microstructural heterogeneity induced by the welding thermal cycle, (weld zone (WZ), heat affected zone (HAZ), and base metal (BM)). Scanning Electron Microscope (SEM) and Energy Dispersive Spectroscopy (EDS) results indicated microstructural coarsening and the formation of numerous large-sized precipitates in the WZ of CHN01 welded joints, which deteriorated its ductility, and thus failed to meet the requirements for jackets of Nb_3Sn conductors. Severe degradation of mechanical properties reveals a critical weakness for CHN01 and similar high-performance alloys: the impressive properties of the BM are not transferable to welded structures, and the effective strengthening mechanisms that make the BM exceptional also make it inherently susceptible to welding embrittlement. Therefore, the future of the CHN01 application hinges not on further enhancing BM properties, but almost exclusively on solving the weldability challenge through innovative filler materials, advanced welding processes, and novel post-weld treatments. The application of CHN01 steel extends beyond thin jacket profiles (3–5 mm) to thick structural components like TF coil cases (up to 300 mm), as illustrated in Figure 3. While progress has been made in qualifying the base material for jackets, the properties of heavy-section forgings remain unsatisfactory, and their weldability is even less understood.

Table 12. Comparison between mechanical properties of the CHN01 base material and welded joint for jacket application (Data from [42]).

	CHN01 Base Material			**CHN01 Welded Joint**		
	300 K	77 K	4.2 K	300 K	77 K	4.2 K
Yield strength ($R_{p0.2}$) (MPa)	546.5	1193.5	1600.0	514.5	1103.0	1335.5
Tensile strength (R_m) (MPa)	776.0	1550.0	1930.0	699.5	1339.0	1622.5
Young's modulus (E) (GPa)	184.0	196.5	215.5	218.5	185.0	219.5
Elongation (e) (%)	49.2	38.5	33.8	29.0	14.5	19.1
Fracture toughness ($K(J)_{Ic}$) (MPa·m$^{1/2}$)			264.5			209.0

To elucidate the failure mechanisms of welded joints, the digital image correlation (DIC) technique was employed, which is an optical, non-contact deformation testing method by analyzing the grayscale patterns of speckle images on the surface of a specimen during the stretching process [117]. Combined with metallographic analysis, DIC mapping of CHN01 welded joints at 6 K localized the cryogenic strain concentration and confirmed that degradation of toughness and plasticity was predominantly confined to the local strain concentration phenomenon in the WZ, which is consistent with previous findings [42,116]. Furthermore, the fracture behavior of the CHN01 base material at 77 K has been systematically investigated using an integrated approach combining mechanical testing and acoustic emission (AE) analysis [118]. AE technique is a highly

sensitive, non-destructive method for the in-situ monitoring of damage evolution in metallic materials [119]. By capturing transient elastic waves generated during crack initiation and propagation, the AE technique provides real-time, multidimensional insights into damage evolution, including localization and identification of damage types [120]. Given that the AE technique has proven effective in characterizing the base material, its application to CHN01 welded joints represents a promising direction, which could monitor the fracture process in the WZ and provide complementary acoustic data to the full-field strain information obtained by the DIC technique, thereby offering a more comprehensive understanding of the failure mechanisms.

5. Comparative Analysis and Future Perspectives

The fracture toughness versus yield strength properties at 4.2 K for structural steels developed by the United States, Japan, and China are compared as summarized in Figure 4. The data reveal a general trend where later-generation materials (indicated by the dotted arrows) achieve a more desirable combination of simultaneously higher strength and greater toughness. JAERI established an early lead with the JJ1 steels in the 1990s, setting a high benchmark for excellent $R_{p0.2}$-K_{Ic} combination (1126 MPa and 366 MPa·m$^{1/2}$), which provided a foundation for their contribution to ITER (JK2LB steel for CS coils) and promoted their current development for JA-DEMO (JN1 steel targeting a higher $R_{p0.2}$ of 1288 MPa). Adopting a more pragmatic approach, the United States firstly explored advanced alloys like INCOLOY 908, which was abandoned owing to its complexity and susceptibility to SAGBO. And the U.S. converged on the well-understood modified 316LN for the jackets of CICCs of TF coils in the ITER, reflecting in its prioritizing manufacturability and reliability over ultimate performance. China's path exemplified an accelerated development. Starting with developing the ITER-grade 316L, China rapidly progressed to indigenously develop CHN01. The CHN01 steel outstands at the forefront of cryogenic mechanical performance by achieving a remarkable $R_{p0.2}$ as 1600 MPa and $K(J)_{Ic}$ as 265 MPa·m$^{1/2}$, making it a leading candidate for the CFETR.

Table 13 underscores an inverse correlation between strength–toughness and manufacturability-weldability. JK2LB of Japan, modified 316LN of the U.S., and modified 316L of China offer relatively excellent weldability and manufacturability, though at different performance levels. Their costs are tied to mature industrial processes. JJ1 of Japan and CHN01 of China, respectively, represent the extreme of cryogenic strength and cryogenic fracture toughness, which could be clearly seen in Figure 4. However, JJ1 steel suffers from severe welding embrittlement requiring special techniques like NG-TIGW while CHN01 steel exhibits significant degradation of strength and toughness in the weld region. The manufacturing of the CHN01 is also inherently difficult, requiring extreme purity control (C and O) and precise thermo-mechanical processing (vacuum oxygen decarbonized and electro-slag remelting), which drastically increases cost and challenges reproducibility for large-scale components. Promotions in cryogenic mechanical performance are often achieved at the expense of weldability and manufacturability, which subsequently raise cost and complicate production. Steel production should be standardized to develop large-scale manufacturing routes and achieve commercialization for huge components in next-generation MCF devices. Implementing comprehensive qualification programs is as important as strictly testing full-scale prototypes under simulated service conditions, including fatigue and electromagnetic loads, to ensure economic viability for fusion energy.

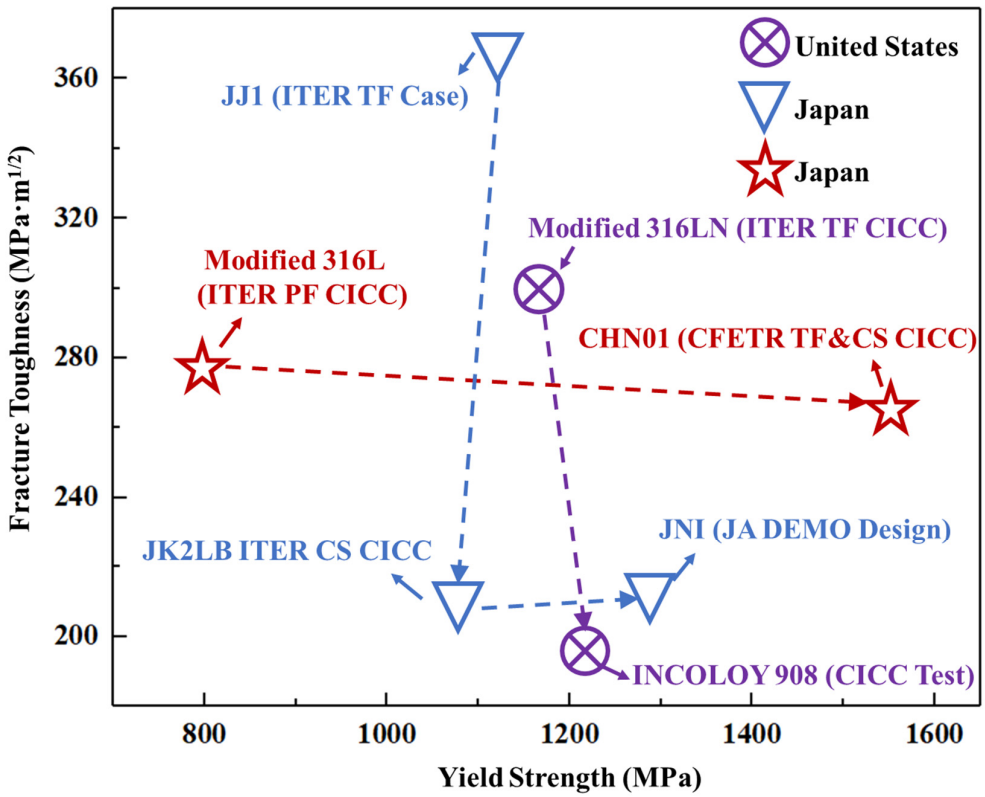


Figure 4. Relationship between fracture toughness and yield strength at 4.2 K of structural steels developed by the United States, Japan and China. (Note: direction of the dotted arrows represents the progression of development time).

Table 13. A comparison of the development of structural steels for coils in Japan, the United States, and China. (Note: the number of stars and squares from the largest to the smallest represents the corresponding performance from excellent to poor).

	Japan			United States		China	
Material	JK2LB	JJ1	JN1	Modified 316LN	INCOLOY 908	Modified 316L	CHN01
Application	ITER CS	ITER TF	JA-DEMO (Design)	ITER TF	CICC Test	ITER PF	CFETR (Design)
Development time	2000s	1990s	2010s	1990s	1990s	2010s	2018
Fracture toughness (MPa·m$^{1/2}$)	209	366	210	300	196	278	265
Yield Strength (MPa)	1076	1126	1288	1165	1216	797	1550
Manufacturability	◊◊◊	◊◊	◊◊	◊◊◊◊	◊	◊◊◊◊	◊◊
Weldability	★★★★	★	★★★	★★★★★	★	★★★★	★★

The research focus for Japan's JN1 and China's CHN01 austenitic stainless steels differs significantly: JN1 emphasizes strengthening base materials, while CHN01 prioritizes anti-embrittlement of welded joints. For JN1 steel, dynamic recrystallization (DRX) techniques could be a promising approach to refine grain structure and reset dislocation densities for simultaneous strength-toughness improvement [121], along with hybrid alloy designs (B/Mo/Nb) that leverage synergistic microalloying effects to overcome conventional trade-offs [113,122,123]; For CHN01 steel, the development of novel filler materials is required. Anti-aging welding materials should be developed by augmenting the concentration of micro-alloy elements that impede weld tissue coarsening, refining the weld grain size, reducing C content in ingots, and enhancing molten steel cleanliness. Furthermore,

residual stresses introduced during manufacturing processes like forging, welding, and cold working can be exacerbated at cryogenic temperatures, potentially accelerating fatigue crack initiation and compromising the structural integrity [124,125]. Post-weld heat treatments and advanced welding techniques are essential to mitigate these stresses. Cryogenic treatment (CT), a supplementary process to conventional heat treatment, has been demonstrated to improve mechanical properties [126] and dimensional stability [127] of ASSs. The process typically involves cooling specimens below −100 °C at a controlled rate, holding for a specified duration, and then reheating. During CT, martensitic transformation can be induced resulting in microstructural refinement, enhanced mechanical properties, and relief of residual stresses in weldments [128–131]. Although current research on cryogenic treatment of CHN01 steel is limited, applying cryogenic treatment to CHN01 welded joints offers a viable pathway to reduce detrimental residual stresses and enhance cryogenic performance via microstructural refinement.

6. Conclusions

Cryogenic high-strength and high-toughness ASSs serve as the critical structural material for superconducting magnet systems in MCF devices. The modified 316LN, JK2LB, and JJ1 steels currently employed in the ITER project have demonstrated reliability under extreme conditions. However, next-generation MCF devices like JA-DEMO and CFETR demand higher mechanical properties, requiring $R_{p0.2}$ exceeding 1500 MPa and $K(J)_{Ic}$ greater than 120 MPa·m$^{1/2}$. Japan focuses on enhancing the fundamental strength of JN1 steel, while China concentrates on resolving performance degradation for CHN01 welded joints which exhibited outstanding $R_{p0.2}$ and $K(J)_{Ic}$ for base material. Future research must prioritize developing novel welding materials by microalloying element addition and improving controlled dynamic recrystallization, along with applying deep cryogenic treatment to enhance the cryogenic performance of WZ in CHN01 welded joints. International collaboration and standardized production will accelerate the transition of these advanced materials from laboratory to engineering applications, ultimately advancing the commercialization of fusion energy.

Author Contributions: Investigation, J.D.; writing—original draft preparation, J.D.; writing—review and editing, C.H.; supervision, C.H. All authors have read and agreed to the published version of the manuscript.

Funding: The development of CHN01 steel has been funded by the National Key R&D Program of China (Grant No.: 2017YFE0301400), and the key Program of the Chinese Academy of Sciences (Grant No.: ZDRW-CN-2021-2-4).

Data Availability Statement: No data was used for the research described in the article.

Conflicts of Interest: The authors declare no conflicts of interest.

Nomenclature

e	Elongation
$K(J)_{Ic}$	Fracture Toughness
R_m	Ultimate Tensile Strength
$R_{p0.2}$	Yield Strength
AE	Acoustic Emission
ASS	Austenitic Stainless Steel
BEST	Burning Experimental Superconducting Tokamak
BM	Base Metal

CC	Correction Coil
CFETR	China Fusion Engineering Test Reactor
CICC	Cable-In-Conduit Conductor
CS	Central Solenoid
DRX	Dynamic Recrystallization
DIC	Digital Image Correlation
EAST	Experimental Advanced Superconducting Tokamak
EBSD	Electron Backscatter Diffraction
ECT	Eddy Current Testing
EDS	Energy Dispersive Spectroscopy
ENEA	European Nuclear Energy Agency
FCC	Face-Centered Cubic
FCGR	Fatigue Crack Growth Rate
FS	Ferritic Steel
HAZ	Heat Affected Zone
HFML	High Field Magnet Laboratory
HMAS	High-Mn Austenitic Steel
HMASS	High-Mn Austenitic Stainless Steel
HTS	High Temperature Superconductivity
INC	International Nickel Corporation
ITER	International Thermonuclear Experimental Reactor
JA-DEMO	Japan Demonstration
JAEA	Japan Atomic Energy Agency
JAERI	Japan Atomic Energy Research Institute
JCS	Japanese Cryogenic Steel
JK2LB	JK2-Low C-B-added
JT-60SA	Japan Torus-60-Super Advanced
LBW	Laser Beam Welding
LEFM	Linear Elastic Fracture Mechanics
MIT	Massachusetts Institute of Technology
NAFASSY	National Facility for Superconducting Systems
NDE	Non-Destructive Examination
NG-MIGW	Narrow-Gap Metal Inert Gas Weld
PAUT	Phased Array Ultrasonic Testing
PF	Polar Field
QST	Quantum Science and Technology
SAGBO	Stress Accelerated Grain Boundary Oxidation
SEM	Scanning Electron Microscope
SFE	Stacking Fault Energy
SHR	Strain Hardening Rate
TEM	Transmission Electron Microscope
TIGW	Tungsten Inert Gas Weld
TF	Toroidal Field
TFTR	Toroidal Fusion Test Reactor
VEBW	Vacuum Electron Beam Weld
WZ	Weld Zone

References

1. International Fusion Research Council (IFRC). Status report on fusion research. *Nucl. Fusion* **2005**, *45*, A1. [CrossRef]
2. Holdren, J.P. Safety and Environmental Aspects of Fusion Energy. *Annu. Rev. Environ. Resour.* **1991**, *16*, 235–258. [CrossRef]
3. Sborchia, C.; Soto, E.B.; Batista, R.; Bellesia, B.; Oliva, A.B.; Rebollo, E.B.; Boutboul, T.; Bratu, E.; Caballero, J.; Cornelis, M.; et al. Overview of ITER magnet system and European contribution. In Proceedings of the 2011 IEEE/NPSS 24th Symposium on Fusion Engineering, Chicago, IL, USA, 26–30 June 2011; pp. 1–8. [CrossRef]

4. Reinders, L.J. The Big Tokamaks: TFTR, JET, JT-60. In *The Fairy Tale of Nuclear Fusion*; Reinders, L.J., Ed.; Springer International Publishing: Cham, Germany, 2021; pp. 183–217. [CrossRef]
5. Tobita, K.; Asakura, N.; Hiwatari, R.; Someya, Y.; Utoh, H.; Katayama, K.; Nishimura, A.; Sakamoto, Y.; Homma, Y.; Kudo, H.; et al. Design Strategy and Recent Design Activity on Japan's DEMO. *Fusion Sci. Technol.* **2017**, *72*, 537–545. [CrossRef]
6. Kwon, S.; Im, K.; Hong, S.-H.; Lee, H.; Rognlien, T.D.; Meyer, W.; Kim, K. Recent progress in the design of the K-DEMO divertor. *Fusion Eng. Des.* **2020**, *159*, 111770. [CrossRef]
7. Zheng, J.; Song, Y.; Liu, X.; Lu, K.; Qin, J. Overview of the Design Status of the Superconducting Magnet System of the CFETR. *IEEE. Trans. Appl. Supercond.* **2018**, *28*, 1–5. [CrossRef]
8. Song, Y.; Li, J.; Wan, Y.; Liu, Y.; Wang, X.; Wan, B.; Fu, P.; Weng, P.; Wu, S.; Duan, X.; et al. Engineering design of the CFETR machine. *Fusion Eng. Des.* **2022**, *183*, 113247. [CrossRef]
9. Jin, H.; Qin, J.G.; Zhou, C.; Liu, H.J.; Liu, F.; Gao, P.; Xiao, G.Y.; Ma, H.J.; Li, J.G.; Wu, Y.; et al. The performance of first CORC cable solenoid insert for development of CFETR high-field magnet. *Nucl. Fusion* **2020**, *60*, 096028. [CrossRef]
10. Dai, C.; Wu, Y.; Li, J.; Guo, Z.; Qin, J.; Long, F.; Nijhuis, A.; Bruzzone, P.; Stepanov, B.; Shi, Y.; et al. Performance test and analysis of the first large-scale cable-in-conduit conductor with high Jc Nb_3Sn strand for fusion reactor. *Nucl. Fusion* **2021**, *61*, 036044. [CrossRef]
11. Watson, J. Mechanical Properties of High-Strength 301 Stainless Steel Sheet at 70, −320, and −423 °F in the Base Metal and Welded Joint Configurations. In *Advances in Cryogenic Engineering: Proceedings of the 1959 Cryogenic Engineering Conference University of California, Berkeley, California September 2–4, 1959*; Springer: Boston, MA, USA, 1960.
12. Libeyre, P.; Bessette, D.; Devred, A.; Jong, C.; Mitchell, N.; Sgobba, S. Conductor jacket development to meet the mechanical requirements of the ITER central solenoid coils. *Fusion Eng. Des.* **2011**, *86*, 1553–1557. [CrossRef]
13. Reed, R.P. Trends and Advances in Cryogenic Materials. In *Cryogenic Engineering*; Timmerhaus, K.D., Reed, R.P., Eds.; Springer: New York, NY, USA, 2007; pp. 52–83. [CrossRef]
14. Mitchell, N.; Devred, A. The ITER magnet system: Configuration and construction status. *Fusion Eng. Des.* **2017**, *123*, 17–25. [CrossRef]
15. Devred, A.; Backbier, I.; Bessette, D.; Bevillard, G.; Gardner, M.; Jong, C.; Lillaz, F.; Mitchell, N.; Romano, G.; Vostner, A. Challenges and status of ITER conductor production. *Supercond. Sci. Technol.* **2014**, *27*, 044001. [CrossRef]
16. Wu, Y.; Qin, J.G.; Liu, B.; Liu, F.; Liu, H.J.; Long, F.; Jin, H.; Jin, J.; Yang, Z.Y.; Pang, Y.C.; et al. Status of the ITER Conductors in China. *IEEE Trans. Appl. Supercond.* **2016**, *26*, 1–5. [CrossRef]
17. Huguet, M.; Team, I.J.C.; Teams, I.H. Key engineering features of the ITER-FEAT magnet system and implications for the R&D programme. *Nucl. Fusion* **2001**, *41*, 1503. [CrossRef]
18. Xin, J.; Zhang, H.; Sun, W.; Wang, W.; Wu, D.; Lyu, B.; Shen, F.; Fang, Z.; Huang, C.; Li, L. Microstructure evolution of austenitic stainless steels under high-cycle-fatigue loading at deep cryogenic temperature. *Scr. Mater.* **2023**, *226*, 115223. [CrossRef]
19. Li, L.F.; Yang, K.; Rong, L.J. Strengthening mechanism of 316LN stainless steel at cryogenic temperatures. *Adv. Cryog. Eng. ICMC* **2002**, *614*, 165–169. [CrossRef]
20. Fernández-Pisón, P.; Rodríguez-Martínez, J.A.; García-Tabarés, E.; Avilés-Santillana, I.; Sgobba, S. Flow and fracture of austenitic stainless steels at cryogenic temperatures. *Eng. Fract. Mech.* **2021**, *258*, 108042. [CrossRef]
21. Sas, J.; Weiss, K.P.; Jung, A. The Mechanical and material properties of 316LN austenitic stainless steel for the fusion application in cryogenic temperatures. *IOP Conf. Ser. Mater. Sci. Eng.* **2015**, *102*, 012003. [CrossRef]
22. Han, W.; Liu, Y.; Wan, F.; Liu, P.; Yi, X.; Zhan, Q.; Morrall, D.; Ohnuki, S. Deformation behavior of austenitic stainless steel at deep cryogenic temperatures. *J. Nucl. Mater.* **2018**, *504*, 29–32. [CrossRef]
23. Ishio, K.; Hamada, K.; Nakajima, H. Effects of nitrogen, niobium, phosphorous and carbon on the mechanical properties of aged 316LN stainless steels at the cryogenic temperature, 4K. *Tetsu Hagane-J. Iron Steel Inst. Jpn.* **2006**, *92*, 30–35. [CrossRef]
24. Walsh, R.P.; Toplosky, V.J.; McRae, D.; Han, K.; Martovetsky, N.N. Cold Work Study on a 316ln Modified Alloy for the Iter tf Coil Conduit. In *AIP Conference Proceedings*; American Institute of Physics: College Park, MD, USA, 2012; Volume 1435, pp. 63–69.
25. Kim, J.H.; Feng, J. The 4K mechanical properties of modified SS316LN for jacket materials in superconducting fusion magnets. In *AIP Conference Proceedings*; American Institute of Physics: College Park, MD, USA, 2008; Volume 54, pp. 92–99.
26. Park, S.H.; Kim, J.Y.; Park, W.W.; Choi, H.; Ma, Y.J.; Kwon, S.P.; Kim, K.; Kang, S.C.; Lee, D.H. The Effect of Plastic Deformation on Low Temperature Mechanical and Magnetic Properties of Austenite 316LN Tube for ITER TF Conductor. *IEEE Trans. Appl. Supercond.* **2012**, *22*, 7800204. [CrossRef]
27. Jin, H.; Wu, Y.; Liu, H.; Han, Q. Mechanical Properties of 316LN Stainless Steel Tube for ITER TF Jacket. *J. Iron Steel Res.* **2012**, *24*, 34–38.
28. Huang, C.; Li, L.; Wu, Z.; Huang, R.; Li, J.; Li, S.; Qin, J.; Liu, H.; Wu, Y. Effect of Solution Annealing Treatment on the Cryogenic Elongation of ITER TF jacket Material-316LN. *Chin. J. Low Temp. Phys.* **2013**, *35*, 117–121.

29. Summers, L.T.; Walsh, R.P.; Miller, J.R. The Cryogenic Tensile and Fracture Toughness Properties of Austenitic Steels Given Low Temperature, Short-Time Nb3Sn Reaction Heat Treatments. In *Advances in Cryogenic Engineering Materials*; Summers, L.T., Ed.; Springer: Boston, MA, USA, 1997; pp. 339–344. [CrossRef]
30. Vostner, A.; Pong, I.; Bessette, D.; Devred, A.; Sgobba, S.; Jung, A.; Weiss, K.P.; Jewell, M.C.; Liu, S.; Yu, W.; et al. Benchmarking of Mechanical Test Facilities Related to ITER CICC Steel Jackets. *IEEE Trans. Appl. Supercond.* **2013**, *23*, 9500705. [CrossRef]
31. Dornfeld, D. Application of acoustic emission techniques in manufacturing. *NDT E Int.* **1992**, *25*, 259–269. [CrossRef]
32. Wu, S.; Xin, J.; Xie, W.; Zhang, H.; Huang, C.; Wang, W.; Zhou, Z.; Zhou, Y.; Li, L. Mechanical properties and microstructure evolution of cryogenic pre-strained 316LN stainless steel. *Cryogenics* **2022**, *121*, 103388. [CrossRef]
33. Anashkin, O.P.; Keilin, V.E.; Krivykh, A.V.; Diev, D.N.; Dinisilov, A.S.; Shcherbakov, V.I.; Tronza, V.I. Tensile Tests of ITER TF Conductors Jacket Materials. In *AIP Conference Proceedings*; American Institute of Physics: College Park, MD, USA, 2012; Volume 1435, pp. 117–124. [CrossRef]
34. Vogt, J.B.; Foct, J.; Regnard, C.; Robert, G.; Dhers, J. Low-temperature fatigue of 316L and 316LN austenitic stainless steels. *Metall. Trans. A.* **1991**, *22*, 2385–2392. [CrossRef]
35. Ogawa, Y.; Okazaki, S.; Takakuwa, O.; Matsunaga, H. The roles of internal and external hydrogen in the deformation and fracture processes at the fatigue crack tip zone of metastable austenitic stainless steels. *Scr. Mater.* **2018**, *157*, 95–99. [CrossRef]
36. Gao, S.; Bai, Y.; Zheng, R.; Tian, Y.; Mao, W.; Shibata, A.; Tsuji, N. Mechanism of huge Lüders-type deformation in ultrafine grained austenitic stainless steel. *Scr. Mater.* **2019**, *159*, 28–32. [CrossRef]
37. Yang, W.H.; Cheng, P.M.; Li, Y.; Wang, R.; Liu, G.; Xin, L.; Zhang, J.Y.; Sun, J. *Ratcheting-induced twinning/de-twinning behaviors in a* 316LN austenitic stainless steel. *Mater. Sci. Eng. A* **2022**, *851*, 143648. [CrossRef]
38. Yang, H.H.; Wu, Z.X.; Huang, C.J.; Huang, R.J.; Li, S.P.; Li, L.F. Stress-induced Martensitic Transformation During Tensile Test of Full-size TF Conductor Jacket Tube at 4.2 K. In *AIP Conference Proceedings*; American Institute of Physics: College Park, MD, USA, 2014; Volume 1574, pp. 48–53. [CrossRef]
39. Yang, H.; Zhang, H.; Xu, X.; Liu, Q.; Li, L. Analysis on full-size ITER TF jacked tubes after tensile test at 300, 77 and 4.2 K. In Proceedings of the 25th International Cryogenic Engineering Conference and International Cryogenic Materials Conference 2014, Enschede, the Netherlands, 7–11 July 2014; Volume 67, pp. 1022–1027. [CrossRef]
40. Devred, A.; Backbier, I.D.; Bessette, G.; Bevillard, M.; Gardner, M.; Jewell, N.; Mitchell, I.P.; Vostner, A. Status of ITER Conductor Development and Production. *IEEE Trans. Appl. Supercond.* **2012**, *22*, 4804909. [CrossRef]
41. Li, X.B.; Jin, H.; Qin, J.G.; Wu, Y.; Li, L.; Wang, K.; Ji, H.; Liu, S. Mechanical Properties of ITER CICC Jacket in China. *IEEE Trans. Appl. Supercond.* **2018**, *28*, 1–5. [CrossRef]
42. Wang, W.; Jin, J.; Wu, L.; Deng, M.; Shi, J.; Jin, H.; Huang, C.; Yuan, Y.; Liu, K.; Wang, S.; et al. Study on the welding properties of modified N50 CICC jacket for future fusion applications. *J. Mater. Res. Technol.* **2023**, *27*, 6094–6103. [CrossRef]
43. Saito, T.; Kawano, K.; Yamazaki, T.; Ozeki, H.; Isono, T.; Hamada, K.; Devred, A.; Vostner, A. Mechanical properties of high manganese austenitic stainless steel JK2LB for ITER central solenoid jacket material. In Proceedings of the 25th International Cryogenic Engineering Conference and International Cryogenic Materials Conference 2014, Enschede, The Netherlands, 7–11 July 2014; Volume 67, pp. 1016–1021. [CrossRef]
44. Sgobba, S.; Dalin, J.-M.; Libeyre, P.; Marcinek, D.J.; Nyilas, A. Progress in Production and Qualification of Stainless Steel Jacket Material for the Conductor of the ITER Central Solenoid. *IEEE Trans. Appl. Supercond.* **2012**, *22*, 7800104. [CrossRef]
45. Sgobba, S.; Libeyre, P.; Marcinek, D.J.; Nyilas, A. A comparative assessment of metallurgical and mechanical properties of two austenitic stainless steels for the conductor jacket of the ITER Central Solenoid. *Fusion Eng. Des.* **2013**, *88*, 2484–2487. [CrossRef]
46. Walsh, R.P.; Han, K.; Toplosky, V.J.; Martovetsky, N.N.; Mann, T.L., Jr.; Miller, J.R. Mechanical Properties of Modified JK2LB for Nb3sn CICC Applications. In *AIP Conference Proceedings*; American Institute of Physics: College Park, MD, USA, 2010; Volume 1219, pp. 17–24. [CrossRef]
47. Feng, J.; Kim, J.; Ballinger, R.G.; Minervini, J.V. Mechanical Properties of JK2LB at 4K. In *AIP Conference Proceedings*; American Institute of Physics: College Park, MD, USA, 2006; Volume 824, pp. 192–199. [CrossRef]
48. Hamada, K.; Nakajima, H.; Kawano, K.; Takano, K.; Tsutsumi, F.; Seki, S.; Okuno, K.; Fujitsuna, N.; Mizoguchi, M. Demonstration of JK2LB jacket fabrication for ITER Central Solenoid. *IEEE Trans. Appl. Supercond.* **2006**, *16*, 787–790. [CrossRef]
49. Ozeki, H.; Saito, T.; Kawano, K.; Takahashi, Y.; Nunoya, Y.; Yamazaki, T.; Isono, T. Effect of Change of Aging Heat Treatment Pattern on the JK2LB Jacket for the ITER Central Solenoid. *Phys. Procedia.* **2015**, *67*, 1010–1015. [CrossRef]
50. Nakajima, H.; Hamada, K.; Takano, K.; Okuno, K.; Fujitsuna, N. Development of low carbon and boron added 22Mn-13Cr-9Ni-1Mo-0.24N steel (JK2LB) for jacket which undergoes Nb/sub 3/Sn heat treatment. *IEEE Trans. Appl. Supercond.* **2004**, *14*, 1145–1148. [CrossRef]
51. Hamada, K.; Nakajima, H.; Kawano, K.; Takano, K.; Tsutsumi, F.; Okuno, K.; Suzuki, T.; Fujitsuna, N. Optimization of JK2LB chemical composition for ITER Central Solenoid conduit material. *Cryogenics* **2007**, *47*, 174–182. [CrossRef]

52. Ishio, K.; Nakajima, H.; Kawasaki, T.; Uehara, S.; Shimamoto, S. Mechanical properties of 110mm thick hot rolled plates of JJ1 and JK2 for ITER TF coil. *Proc. Inter. Conf. Magnet Tech.* **1997**, 989–992. Available online: https://jopss.jaea.go.jp/search/servlet/search?2001518&language=1 (accessed on 10 October 2025).
53. Libeyre, P.; Mitchell, N.; Bessette, D.; Gribov, Y.; Jong, C.; Lyraud, C. Detailed design of the ITER central solenoid. *Fusion Eng. Design* **2009**, *84*, 1188–1191. [CrossRef]
54. Walsh, R.P.; McRae, D.M.; Han, K.; Martovetsky, N.N. Tensile and fatigue qualification testing of ITER-CS conduit alloy JK2LB. *IOP Conf. Ser. Mater. Sci. Eng.* **2015**, *102*, 012002. [CrossRef]
55. Lu, J.; Walsh, R.P.; Han, K. Low temperature physical properties of a high Mn austenitic steel JK2LB. *Cryogenics* **2009**, *49*, 133–137. [CrossRef]
56. Takahashi, Y.; Suwa, T.; Nabara, Y.; Ozeki, H.; Hemmi, T.; Nunoya, Y.; Isono, T.; Matsui, K.; Kawano, K.; Oshikiri, M.; et al. Non-Destructive Examination of Jacket Sections for ITER Central Solenoid Conductors. *IEEE Trans. Appl. Supercond.* **2015**, *25*, 1–4. [CrossRef]
57. Ozeki, H.; Hamada, K.; Takahashi, Y.; Nunoya, Y.; Kawano, K.; Oshikiri, M.; Saito, T.; Teshima, O.; Matsunami, M. Establishment of Production Process of JK2LB Jacket Section for ITER CS. *IEEE Trans. Appl. Supercond.* **2014**, *24*, 1–4. [CrossRef]
58. Lim, B.; Simon, F.; Ilyin, Y.; Gung, C.Y.; Smith, J.; Hsu, Y.H.; Luongo, C.; Jong, C.; Mitchell, N. Design of the ITER PF Coils. *IEEE Trans. Appl. Supercond.* **2011**, *21*, 1918–1921. [CrossRef]
59. Qin, J.; Weiss, K.-P.; Wu, Y.; Wu, Z.; Li, L.; Liu, S. Fatigue tests on the ITER PF jacket. *Cryogenics* **2012**, *52*, 486–490. [CrossRef]
60. Liu, H.J.; Wu, Y.; Han, Q.Y.; Wu, Z.X.; Li, L.F. Mechanical tests on the ITER PF 316L jacket after compaction. *Cryogenics* **2011**, *51*, 234–236. [CrossRef]
61. Huang, C.; Huang, R.; Li, L. Mechanical property tests on structural materials for ITER magnet system at low temperatures in China. In *AIP Conference Proceedings*; American Institute of Physics: College Park, MD, USA, 2014; Volume 1574, pp. 346–353. [CrossRef]
62. Liu, X.; Wu, Y.; Qin, J.; Li, L.; Deng, M.; Wang, W.; Pedrosa, N.M.; Sousa, J.P.; Vostner, A.; Devred, A. Developments of Nondestructive Test Method of Jacket Section for ITER Poloidal Field Coils. *IEEE Trans. Appl. Supercond.* **2016**, *26*, 1–4. [CrossRef]
63. Peng, J.; Wu, Y.; Liu, H.; Shi, Y.; Chen, J.; Ren, Z. The cryogenic system for ITER CC superconducting conductor test facility. *Cryogenics* **2011**, *51*, 62–67. [CrossRef]
64. Qin, J.; Weiss, K.-P.; Wu, Y.; Liao, G.; Wu, Z.; Li, L.; Li, H.; Niu, E. Mechanical test on the ITER CC and Feeder jacket. *Fusion Eng. Des.* **2013**, *88*, 151–155. [CrossRef]
65. Suresh, S. *Fatigue of Materials*, 2nd ed.; Cambridge University Press: Cambridge, UK, 1998. [CrossRef]
66. Mitchell, N.; Alekseev, A.; Gallix, R.; Holland, D.; Meyder, R.; Panin, A.; Shimada, M.; Wong, F.; Zapretelina, E. Magnet Safety Assessment for ITER. *J. Fusion Energy* **1997**, *16*, 25–35. [CrossRef]
67. Wong, F.M.G.; Mitchell, N.A. Selection of Tokamak Toroidal Field Coil Case Structural Materials. In *Advances in Cryogenic Engineering Materials*; Balachandran, U.B., Gubser, D.G., Hartwig, K.T., Reed, R.P., Warnes, W.H., Bardos, V.A., Eds.; Springer: Boston, MA, USA, 1998; pp. 65–72. [CrossRef]
68. Iguchi, M.; Sakurai, T.; Nakhira, M.; Koizumi, N.; Nakajima, H. Cryogenic Structural Materials of the ITER Toroidal Field Coil Structure. In *Fourth International Workshop on Structural Materials for Innovative Nuclear Systems (SMINS-4)*; The Nuclear Energy Agency: Paris, France, 2017.
69. Iguchi, M.; Sakurai, T.; Hisashige, T.; Nakahira, M. Evaluation of Mass Production Results of Cryogenic Structural Stainless Steels for ITER Toroidal Field Coils. *IEEE Trans. Appl. Supercond.* **2022**, *32*, 1–5. [CrossRef]
70. Iguchi, M.; Saito, T.; Kawano, K.; Takano, K.; Tsutsumi, F.; Chida, Y.; Nakajima, H. Estimation of Tensile Strengths at 4K of 316LN Forging and Hot Rolled Plate for the ITER Toroidal Field Coils. In *AIP Conference Proceedings*; American Institute of Physics: College Park, MD, USA, 2012; Volume 1435, pp. 70–77. [CrossRef]
71. Iguchi, M.; Saito, T.; Kawano, K.; Chida, Y.; Nakajima, H.; Ogawa, T.; Katayama, Y.; Ogata, H.; Minemura, T.; Tokai, D.; et al. Mechanical properties of full austenitic welding joint at cryogenic temperature for the ITER toroidal field coil structure. *Fusion Eng. Des.* **2013**, *88*, 2520–2524. [CrossRef]
72. Ishio, K.; Nakajima, H.; Nunoya, Y.; Miura, Y.; Kawasaki, T.; Tsuji, H. Trial Fabrication of Heavy Section Base Metals and Welded Joints for ITER TF Coil. In *Advances in Cryogenic Engineering Material*; Balachandran, U.B., Gubser, D.G., Hartwig, K.T., Reed, R.P., Warnes, W.H., Bardos, V.A., Eds.; Springer: Boston, MA, USA, 1998; pp. 73–80. [CrossRef]
73. Onozuka, M.; Shimizu, K.; Urata, K.; Kimura, M.; Kadowaki, H.; Okamoto, M.; Nakajima, H.; Hamada, K.; Okuno, K. Basic analysis of weldability and machinability of structural materials for ITER Toroidal Field coils. *Fusion Eng. Des.* **2007**, *82*, 1431–1436. [CrossRef]
74. Shindo, Y.; Kobori, T.; Horiguchi, K.; Yamada, E.; Nakajima, H.; Tsuji, H. Fracture toughness and temperature rise during crack propagation in forged JJ1 type austenitic stainless steel plate at 4.2 K. *Nippon. Kinzoku Gakkaishi (J. Jpn. Inst. Met.)* **1995**, *59*, 793–798.

75. Shindo, Y.; Takahashi, T.; Horiguchi, K.; Sanada, K.; Kobori, T. Cryogenic fracture toughness and temperature rise of thick section weldments in forged JJ1 type austenitic stainless steel plate. *Weld. Int.* **1998**, *12*, 360–365. [CrossRef]
76. Hamada, K.; Nakajima, H.; Kawano, K.; Takano, K.; Tsutsumi, F.; Okuno, K. Demonstration of full scale JJ1 and 316LN fabrication for ITER TF coil structure. *Fusion Eng. Des.* **2007**, *82*, 1481–1486. [CrossRef]
77. Hamada, K.; Nakajima, H.; Takano, K.; Kudo, Y.; Tsutsumi, F.; Okuno, K.; Jong, C. Fatigue assessment of the ITER TF coil case based on JJ1 fatigue tests. *Fusion Eng. Des.* **2005**, *75*, 87–91. [CrossRef]
78. Fang, C.; Song, Y.; Wei, J.; Xin, J.; Wu, H.; Handroos, H.; Salminen, A.; Li, H.; Libeyre, P.; Dolgetta, N. Microstructural characteristics of the laser welded joint of ITER correction coil sub case. *Fusion Eng. Des.* **2015**, *98–99*, 1960–1963. [CrossRef]
79. Foussat, A.; Wu, W.; Li, H.; Dolgetta, N.; Libeyre, P.; Mitchell, N. Qualification Phase of Key Technologies for ITER Correction Coils. *IEEE Trans. Appl. Supercond.* **2012**, *22*, 4201205. [CrossRef]
80. Xin, J.; Fang, C.; Song, Y.; Wei, J.; Huang, C.; Libeyre, P.; Simon, F.; Sgobba, S. Microstructure and Mechanical Properties of ITER Correction Coil Case Material. *IEEE Trans. Appl. Supercond.* **2017**, *27*, 1–8. [CrossRef]
81. Foussat, A.; Wu, W.; Jing, W.; Du, S.; Sgobba, S.; Li, H.; Libeyre, P.; Jong, C.; Klofac, K.; Mitchell, N. Mechanical design and construction qualification program on ITER correction coils structures. *Nucl. Eng. Des.* **2014**, *269*, 116–124. [CrossRef]
82. Wei-yue, W. Structure analysis of correction coils for ITER. *Nucl. Fusion Plasma Phys.* **2009**, *29*, 264.
83. Foussat, A.; Dolgetta, N.; Jong, C.; Libeyre, P.; Mitchell, N.; Wu, W.; Liu, L.; Du, S.; Liu, X.; Yu, X.; et al. From Design to Development Phase of the ITER Correction Coils. *IEEE Trans. Appl. Supercond.* **2011**, *21*, 1960–1963. [CrossRef]
84. Foussat, A.; Libeyre, P.; Mitchell, N.; Gribov, Y.; Jong, C.T.J.; Bessette, D.; Gallix, R.; Bauer, P.; Sahu, A. Overview of the ITER Correction Coils Design. *IEEE Trans. Appl. Supercond.* **2010**, *20*, 402–406. [CrossRef]
85. Fang, C.; Song, Y.; Wu, W.; Wei, J.; Zhang, S.; Li, H.; Dolgetta, N.; Libeyre, P.; Cormany, C.; Sgobba, S. *The Laser Welding with Hot Wire of* 316LN Thick Plate Applied on ITER Correction Coil Case. *J. Fusion Energy* **2014**, *33*, 752–758. [CrossRef]
86. Huang, C.; Xin, J.; Wei, J.; Zhang, H.; Huang, R.; Xu, D.; Liu, S.; Li, L. Assessment of Mechanical Properties of Welding Joints for ITER Correction Coils Cases at Cryogenic Temperature. *IEEE Trans. Appl. Supercond.* **2021**, *31*, 1–5. [CrossRef]
87. Zhou, Z.; Wu, W.; Wei, J.; Du, S.; Han, S.; Liu, L.; Yu, X.; Li, H.; Foussat, A.; Libeyre, P. Research on Manufacture and Enclosure Welding of ITER Correction Coils Cases. *IEEE Trans. Appl. Supercond.* **2012**, *22*, 4202603. [CrossRef]
88. De Cooman, B.C. 11-High Mn TWIP steel and medium Mn steel. In *Automotive Steels*; Rana, R., Singh, S.B., Eds.; Woodhead Publishing: Cambridge, UK, 2017; pp. 317–385. [CrossRef]
89. Lu, J.; Hultman, L.; Holmström, E.; Antonsson, K.H.; Grehk, M.; Li, W.; Vitos, L.; Golpayegani, A. Stacking fault energies in austenitic stainless steels. *Acta Mater.* **2016**, *111*, 39–46. [CrossRef]
90. Curtze, S.; Kuokkala, V.T. Dependence of tensile deformation behavior of TWIP steels on stacking fault energy, temperature and strain rate. *Acta Mater.* **2010**, *58*, 5129–5141. [CrossRef]
91. Shimamoto, S.; Nakajima, H.; Yoshida, K.; Tada, E. Requirements for Structural Alloys for Superconducting Magnet Cases. In *Advances in Cryogenic Engineering Materials*; Reed, R.P., Clark, A.F., Eds.; Springer: Boston, MA, USA, 1986; pp. 23–32. [CrossRef]
92. Umezawa, O. Review of the Mechanical Properties of High-Strength Alloys at Cryogenic Temperatures. *Mater. Perform. Charact.* **2021**, *10*, 20200138. [CrossRef]
93. Nakajima, H.; Yoshida, K.; Shimamoto, S. Development of the Fusion of New Cryogenic Steels Experimental Reactor for the Superconducting Magnets. *ISIJ Int.* **2001**, *30*, 567–578. [CrossRef]
94. Hwang, I.S.; Ballinger, R.G.; Morra, M.M.; Steeves, M.M. Mechanical Properties of Incoloy 908—An Update. In *Materials*; Fickett, F.R., Reed, R.P., Eds.; Springer: Boston, MA, USA, 1992; pp. 1–10. [CrossRef]
95. Wang, W.; Zhao, C.; Jin, J.; Shi, J.; Tu, Z.; Chen, X.; Huang, C.; Li, L.; Li, J.; Qin, J. The research on high-strength CICC jackets with YS > 1500 MPa at 4.2 K for future fusion applications. *Nucl. Mater. Energy* **2023**, *36*, 101474. [CrossRef]
96. Yong-Hwan, K.; Sang-He, K.; Young-Hwan, K.; Han-Sung, K.; Kie-Hyung, C. Mechanical analysis of the KSTAR CS model coil. *IEEE Trans. Appl. Supercond.* **1999**, *9*, 228–231. [CrossRef]
97. Lim, B.S.; Lee, S.-I.; Kim, K.; Choi, J.Y. Fabrication of the KSTAR superconducting CICC. *IEEE Trans. Appl. Supercond.* **2002**, *12*, 591–594. [CrossRef]
98. Libeyre, P.; Brosset, C.; Decool, P.; Rubino, M.; Bevilacqua, G.; Laurenti, A.; Pesenti, P.; Ursuleac, M.; Valle, N.; Nyilas, A. Risks and benefits of Incoloy 908. *Fusion Eng. Des.* **2001**, *58–59*, 129–134. [CrossRef]
99. Okano, K.; Kasada, R.; Ikebe, Y.; Ishii, Y.; Oba, K.; Kashiwagi, M.; Sakamoto, R.; Sawa, N.; Takenaga, H.; Nishimura, A.; et al. An action plan of Japan toward development of demo reactor. *Fusion Eng. Des.* **2018**, *136*, 183–189. [CrossRef]
100. Tobita, K.; Utoh, H.; Hiwatari, R.; Miyoshi, Y.; Tokunaga, S.; Sakamoto, Y.; Someya, Y.; Asakura, N.; Homma, Y.; Nakajima, N.; et al. Conceptual design of Japan's fusion DEMO reactor (JADEMO) and superconducting coil issues. *J. Phys. Conf. Ser.* **2019**, *1293*, 012078. [CrossRef]
101. Nakajima, H.; Yoshida, K.; Shimamoto, S. Development of New Cryogenic Steels for the Superconducting Magnets of the Fusion Experimental Reactor. *ISIJ Int.* **1990**, *30*, 567–578. [CrossRef]

102. Nakajima, H.; Takano, K.; Tsutsumi, F.; Kawano, K.; Hamada, K.; Okuno, K. Qualification of Cryogenic Structural Materials for the ITER Toroidal Field Coils. In Proceedings of the ASME 2009 Pressure Vessels and Piping Conference, Prague, Czech Republic, 26–30 July 2009; pp. 789–797. [CrossRef]
103. Nakajima, H.; Hamada, K.; Okuno, K.; Hada, K.; Tada, E. New cryogenic material and design for ITER superconducting magnet system. In Proceedings of the 10th International Conference on Nuclear Engineering, Arlington, VA, USA, 14–18 April 2002; pp. 591–598.
104. Utoh, H.; Sakamoto, Y.; Miura, H.; Arakawa, H.; Echizenya, D.; Matsuda, T.; Hasegawa, M.; Nomoto, K. Design study of superconducting coil system for JA DEMO. *Fusion Eng. Des.* **2024**, *202*, 114345. [CrossRef]
105. Zhuang, G.; Li, G.Q.; Li, J.; Wan, Y.X.; Liu, Y.; Wang, X.L.; Song, Y.T.; Chan, V.; Yang, Q.W.; Wan, B.N.; et al. Progress of the CFETR design. *Nucl. Fusion.* **2019**, *59*, 112010. [CrossRef]
106. Yao, C.; Ma, Y. Superconducting materials: Challenges and opportunities for large-scale applications. *iScience.* **2021**, *24*, 102541. [CrossRef]
107. Zheng, J.; Song, Y.; Liu, F.; Liu, X.; Lu, K.; Zhu, L.; Xu, W.; Shen, G.; Fang, C.; Li, C.; et al. Progress in engineering design of CFETR toroidal field superconducting magnet. *Fusion Eng. Des.* **2022**, *177*, 113063. [CrossRef]
108. Langeslag, S.A.E.; Sgobba, S.; Libeyre, P.; Marcinek, D.J.; Zhang, Z. Extensive characterisation of advanced manufacturing solutions for the ITER Central Solenoid pre-compression system. *Fusion Eng. Des.* **2015**, *98–99*, 2015–2019. [CrossRef]
109. McRae, D.M.; Walsh, R.P.; Dalder, E.N.C.; Litherland, S.; Trosen, M.; Kuhlmann, D.J. Fatigue and fracture properties of a super-austenitic stainless steel at 295 K and 4 K. In *AIP Conference Proceedings*; American Institute of Physics: College Park, MD, USA, 2014; Volume 1574, pp. 59–66. [CrossRef]
110. Libeyre, P.; Cormany, C.; Dolgetta, N.; Gaxiola, E.; Jong, C.; Lyraud, C.; Reiersen, W.; Everitt, D.; Martovetsky, N.; Rosenblad, P.; et al. Status of design and manufacturing of the ITER Central Solenoid and Correction Coils. In Proceedings of the 2015 IEEE 26th Symposium on Fusion Engineering (SOFE), Austin, TX, USA, 31 May–4 June 2015; pp. 1–8. [CrossRef]
111. Zhai, R.; Zhang, H.; Xu, B.; Liu, S.; Xie, B.; Sun, M. Elimination of δ-ferrite in N50 steel and its effect on cryogenic mechanical properties. *Cryogenics* **2022**, *126*, 103522. [CrossRef]
112. Zhai, R.; Zhang, H.; Liu, S.; Sun, M.; Sheng, S.; Xu, B. Influence of carbon content on the microstructure and cryogenic tensile properties of N50 austenitic stainless steel after aging treatment. *J. Nucl. Mater.* **2022**, *571*, 154023. [CrossRef]
113. Zhai, R.; Zhang, H.; Pan, S.; Xu, B.; Liu, S.; Sun, M. Effect of boron addition on the microstructure and cryogenic mechanical properties of N50 stainless steel after aging treatment. *Mater. Sci. Eng. A.* **2023**, *881*, 145372. [CrossRef]
114. Zhai, R.; Zhang, H.; Qi, X.; Wang, W.; Chen, X.; Xu, B.; Sun, M. Fabrication and performance evaluation of CICC jacket based on modified N50 austenitic steel for CFETR magnet. *J. Mater. Res. Technol.* **2024**, *28*, 3435–3448. [CrossRef]
115. Wang, W.; Zhao, C.; Jin, H.; Huang, C.; Li, L.; Tu, Z.; Xu, B.; Zhai, R.; Li, J.; Qin, J. Mechanical properties evaluation of ReBCO CICC jacket based on super-austenitic stainless steel for CFETR high-field magnet. *Nucl. Mater. Energy.* **2023**, *34*, 101344. [CrossRef]
116. Dai, J.; Xie, L.; Wang, W.; Xin, J.; Li, B.; Bao, R.; Huang, Y.; Huang, C.; Sun, W.; Wang, W.; et al. Evaluation of localized mechanical properties of modified N50 welded joints at cryogenic temperature through a digital image correlation technique. *Cryogenics* **2024**, *143*, 103960. [CrossRef]
117. Pan, B. Recent Progress in Digital Image Correlation. *Exp. Mech.* **2011**, *51*, 1223–1235. [CrossRef]
118. Zhang, B.; Bao, R.; Dai, J.; Sun, W.; Huang, C.; Shi, L.; Zhao, Y.; Zhou, H.; Zheng, W.; Li, L.; et al. Recognition of fracture stages of CHN01 austenitic stainless steel by acoustic emission at cryogenic temperature. *Cryogenics* **2025**, *150*, 104154. [CrossRef]
119. Moorthy, V.; Jayakumar, T.; Raj, B. Acoustic emission behaviour during stage II fatigue crack growth in an AISI type 316 austenitic stainless steel. *Bull. Mater. Sci.* **1994**, *17*, 699–715. [CrossRef]
120. Sawan, H.A.; Walter, M.E.; Marquette, B. Unsupervised learning for classification of acoustic emission events from tensile and bending experiments with open-hole carbon fiber composite samples. *Compos. Sci. Technol.* **2015**, *107*, 89–97. [CrossRef]
121. Huang, K.; Logé, R.E. A review of dynamic recrystallization phenomena in metallic materials. *Mater. Des.* **2016**, *111*, 548–574. [CrossRef]
122. Seol, J.B.; Bae, J.W.; Kim, J.G.; Sung, H.; Li, Z.; Lee, H.H.; Shim, S.H.; Jang, J.H.; Ko, W.-S.; Hong, S.I.; et al. Short-range order strengthening in boron-doped high-entropy alloys for cryogenic applications. *Acta. Mater.* **2020**, *194*, 366–377. [CrossRef]
123. Uranga, P.; Shang, C.J.; Senuma, T.; Yang, J.R.; Guo, A.M.; Mohrbacher, H. Molybdenum alloying in high-performance flat-rolled steel grades. *Adv. Manuf.* **2020**, *8*, 15–34. [CrossRef]
124. Miyazaki, T.; Sasaki, T. X-Ray Residual Stress Measurement of Austenitic Stainless Steel Based on Fourier Analysis. *Nucl. Technol.* **2016**, *194*, 111–116. [CrossRef]
125. Kim, J.S.; Kim, M.W.; Yang, J.S. Investigation on effect of thermal aging embrittlement on residual stresses of austenitic stainless steel repair welds in nuclear components subject to seismic loads. *J. Mech. Sci. Technol.* **2020**, *34*, 2821–2831. [CrossRef]
126. Weng, Z.; Gu, K.; Wang, K.; Liu, X.; Wang, J. The reinforcement role of deep cryogenic treatment on the strength and toughness of alloy structural steel. *Mater. Sci. Eng. A* **2020**, *772*, 138698. [CrossRef]

127. Weng, Z.; Liu, X.; Gu, K.; Guo, J.; Cui, C.; Wang, J. Modification of residual stress and microstructure in aluminium alloy by cryogenic treatment. *Mater. Sci. Technol.* **2020**, *36*, 1547–1555. [CrossRef]
128. Kalia, S. Cryogenic Processing: A Study of Materials at Low Temperatures. *J. Low Temp. Phys.* **2010**, *158*, 934–945. [CrossRef]
129. Shokrani, A.; Dhokia, V.; Muñoz-Escalona, P.; Newman, S.T. State-of-the-art cryogenic machining and processing. *Int. J. Comput. Integr. Manuf.* **2013**, *26*, 616–648. [CrossRef]
130. Cui, C.; Gu, K.; Qiu, Y.; Weng, Z.; Zhang, M.; Wang, J. The effects of post-weld aging and cryogenic treatment on self-fusion welded austenitic stainless steel. *J. Mater. Res. Technol.* **2022**, *21*, 648–661. [CrossRef]
131. Cui, C.; Weng, Z.; Gu, K.; Zhang, M.; Wang, J.; Zhang, Y. The strengthening role of post-welded cryogenic treatment on the performance and microstructure of 304 austenitic stainless steel weldments. *J. Mater. Res. Technol.* **2024**, *29*, 5576–5584. [CrossRef]

Disclaimer/Publisher's Note: The statements, opinions and data contained in all publications are solely those of the individual author(s) and contributor(s) and not of MDPI and/or the editor(s). MDPI and/or the editor(s) disclaim responsibility for any injury to people or property resulting from any ideas, methods, instructions or products referred to in the content.